Magnetic interactions in cubic-, hexagonal- and trigonal barium iron oxide fluoride, BaFeO2F

CLEMENS, Oliver, MARCO, Jose F., THOMAS, Michael F., FORDER, Sue, ZHANG, Hongbin, CARTENET, Simon, MONZE, Anais, BINGHAM, Paul A. <http://orcid.org/0000-0001-6017-0798>, SLATER, Peter R. and BERRY, Frank J.

Published version

CLEMENS, Oliver, MARCO, Jose F., THOMAS, Michael F., FORDER, Sue, ZHANG, Hongbin, CARTENET, Simon, MONZE, Anais, BINGHAM, Paul A., SLATER, Peter R. and BERRY, Frank J. (2016). Magnetic interactions in cubic-, hexagonal- and trigonal barium iron oxide fluoride, BaFeO2F. Journal of Physics: Condensed Matter, 28 (34).

Magnetic interactions in cubic-, hexagonal- and trigonal-barium iron oxide fluoride, $BaFeO_2F$

Oliver Clemens[a,b,c], José F. Marco[d], Michael F. Thomas[e], Susan D. Forder[f], Hongbin Zhang[g], Simon Cartenet[f] , Anais Monze[f] , Paul A. Bingham[f] , Peter R. Slater[a], Frank J. Berry[a,*]

[a] School of Chemistry, The University of Birmingham, Birmingham B15 2TT, United Kingdom.

[b] Technical University of Darmstadt, Joint Research Laboratory Nanomaterials, Jovanka-Bontschits-Straße 2, 64287 Darmstadt, Germany.

[c] Karlsruhe Institute of Technology, Institute of Nanotechnology, Hermann-von-Helmholtz-Platz 1, 76344 Eggenstein-Leopoldshafen, Germany.

[d] Instituto de Quimica-Fisica,“Rocasolano”, CSIC, Serrano 119, 28006 Madrid, Spain.

[e] Department of Physics, University of Liverpool, Liverpool L69 3BX, United Kingdom.

[f] Materials and Engineering Research Institute, Sheffield Hallam University, Sheffield S1 1WB, United Kingdom.

[g] Technical University of Darmstadt, Theory of Magnetic Materials, Jovanka-Bontschits-Straße 2, 64287 Darmstadt, Germany.

*: corresponding author

Fax +44 (0)121 4144403

Email f.j.berry.1@bham.ac.uk

Abstract

^{57}Fe Mössbauer spectra have been recorded from the hexagonal (6H)- and trigonal (15R)- modifications of $BaFeO_2F$ and are compared with those previously recorded from the cubic form of $BaFeO_2F$. The spectra, recorded over a temperature range from 15 to 650K show that all of the iron in all the compounds is in the Fe^{3+} state. Spectra from the 6H- and 15R- modifications were successfully fitted with components that were related to the Fe(1) and Fe(2) structural sites in the 6H variant and to the Fe(1), Fe(2) and Fe(3) structural sites in the 15R form. The magnetic ordering temperatures were determined as 597±3K for 6H-$BaFeO_2F$ and 636±3K for 15R-$BaFeO_2F$. These values are surprisingly close to the value of 645±5K determined for the cubic form. The magnetic interactions in the three forms are compared with a view to explaining this similarity of magnetic ordering temperature.

Keywords

Mössbauer spectra, magnetic ordering temperature, superexchange.

1 Introduction

Perovskite-related oxide fluorides have attracted significant interest since the observation of superconductivity in $Sr_2CuO_2F_{2+d}$ [1-4]. We have been particularly interested in the synthesis, structural- and magnetic- characterisation of fluorinated cubic perovskite-related structures of composition $MFeO_2F$ (M = Sr, Ba) [5-12] using polyvinylidenedifluoride (PVDF) as a fluorinating agent [13]. More recently, we have reported on the synthesis and structural characterisation of two structurally different modifications of $BaFeO_2F$: hexagonal 6H-$BaFeO_2F$ (space group $P6_3/mmc$ [14]) and trigonal 15R-$BaFeO_2F$ (space group R-3m [15]).

The structures of the $BaFeO_2F$ modifications can be understood in terms of the close packing of BaO_2F layers with iron occupying ¼ of the octahedral sites. If a layer "A" is surrounded by two layers with different orientation (*e.g.* BAC), it is assigned the letter *c* in the Jagodzinski notation whereas if the layer "A" is surrounded by two layers with the same orientation (*e.g.* BAB), it is assigned the letter *h* [16]. For a stapling sequence *ccc*… the simple cubic perovskite structure is formed as found, for example, in $SrFeO_3$ whereas the hexagonal perovskite structure is obtained for the sequence *hhh*….in, for example, $BaCoO_3$. Hence the modifications of $BaFeO_2F$ considered here differ in the stacking sequence of the BaO_2F layers. The respective stacking sequences are *ccc*… for cubic $BaFeO_2F$, *cchcch*… for 6H-$BaFeO_2F$ and *chcchchcchchcch*… for 15R-$BaFeO_2F$. The stacking sequence also determines how the iron octahedra are connected to the neighbouring octahedra. For octahedra connecting via *c*-type layers the octahedron only shares corners with the neighbouring octahedra via this layer. For connection via an *h*-type layer the two octahedra share a common face. An overview of the structures of the three modifications is given in Figure 1. Although the type of modification formed in inorganic compounds is often influenced by the average transition metal oxidation state and the size of the A site cation (here Ba^{2+}), in this work the low temperature fluorination routes have allowed the synthesis of three different perovskite-type structures all containing Fe^{3+} with the same A site cations and identical overall anion composition.

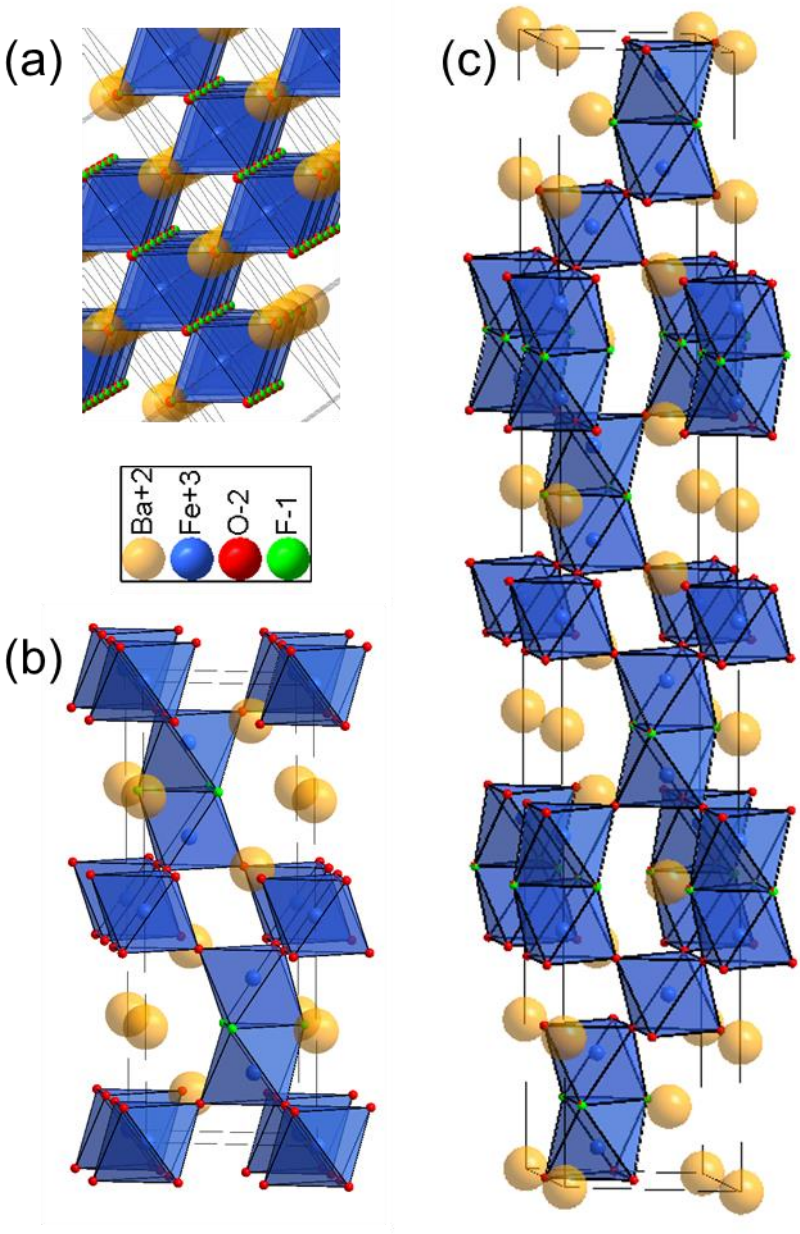

Figure 1. Crystal structures of (a) cubic-, (b) hexagonal 6H- and (c) trigonal 15R-$BaFeO_2F$.

Furthermore, the magnetic structures of the hexagonal- and trigonal- modifications of $BaFeO_2F$ as revealed by neutron powder diffraction are complex [14, 15] and, as might be expected, are different from those identified by neutron powder diffraction and ^{57}Fe Mössbauer spectroscopy in cubic $BaFeO_2F$ [9]. Cubic $BaFeO_2F$ shows G-type antiferromagnetic ordering, i. e. each iron atom possesses spin direction opposite to its nearest neighbours. In 6H- and 15R- $BaFeO_2F$, the spins on neighbouring Fe atoms (i.e. octahedra which are connected by either corner or face) are also aligned antiparallel. In an alternative description, the iron atoms between close packed BaO_2F layers align parallel (the octahedra are not connected to other octahedra of the same layer), but align antiparallel to neighbouring layers. The

magnetic moments are aligned parallel to the *a/b*-plane in both cases, i.e. perpendicular to the stacking direction of BaO_2F layers [14, 15].

We have now recorded ^{57}Fe Mössbauer spectra from both 6H-$BaFeO_2F$ and 15R-$BaFeO_2F$ at temperatures between 630K and 15 K. We report here on these spectra and compare them with data recorded over a similar temperature range from cubic $BaFeO_2F$ [9]. The results are discussed in terms of the different magnetic interactions between the Fe^{3+} ions which originate from the differences in crystal structure.

2 Experimental Details

Cubic perovskite-related $BaFeO_{2.5}$ [17] was prepared by the calcination of appropriate quantities of a well ground mixture of $BaCO_3$ and α-Fe_2O_3 at 1100°C for 24 h in air with one intermediate regrinding. Fluorination was achieved by mixing this compound with PVDF in a 0.60 molar ratio (precursor oxide : CH_2CF_2 unit and equivalent to a 20% excess) and heating the mixture at 375°C for 24 h in air.

Hexagonal 6H-$BaFeO_{3-d}$ was prepared by heating a stoichiometric planetary ball-milled mixture of $BaCO_3$ and α-Fe_2O_3 at 970°C for 12 h under flowing oxygen. The sample was slowly cooled to room temperature to increase the oxygen uptake and the heating procedure was repeated a second time. Fluorination was achieved by mixing the 6H-$BaFeO_{3-d}$ with a 4 % excess of PVDF, grinding in n-pentane, and slowly heating to 370°C (20°C/h) under air for 20 h.

Trigonal 15R-$BaFeO_2F$ was prepared by heating a stoichiometric planetary ball-milled mixture of BaF_2, $BaCO_3$ and α-Fe_2O_3, which had been pressed into a pellet, at 900°C for 12 h under air in a covered alumina crucible. The product was quenched to room temperature to give a precursor oxide of composition 15R-$BaFeO_{3-d}F_{0.2}$ (as reported in [18, 19]). 15R-$BaFeO_2F$ was prepared by grinding 15R-$BaFeO_{3-d}F_{0.2}$ and a 4 % excess of PVDF in n-pentane and slowly heating the mixture to 370°C at 20°C/h under air. The sample was maintained at 370°C for 20 h.

^{57}Fe Mössbauer spectra were recorded with a constant acceleration spectrometer in transmission geometry using a ca. 25 mCi ^{57}Co/Rh source and a helium closed-cycle cryorefrigerator. For temperatures above room temperature a furnace sample chamber was used using thermocouple temperature control. All spectra were

computer fitted and the chemical isomer shift data are quoted relative to that of metallic iron at room temperature.

Exchange parameters were estimated using density functional theory (DFT) based on calculations for the fluoride ordered structure of 6H-$BaFeO_2F$ ($P6_3/mmc$). DFT calculations were performed using the full potential linear augmented planewave method as implemented in the Wien2k code [20]. The exchange-correlation potentials are approximated using the local spin density functional as parameterized [21]. The self-consistent calculations were carried out with RMT*KMAX of 7.0 on a k-mesh of 13×13×4 to guarantee good convergence. The exchange parameters were estimated using the energy mapping methods, where the total energies between experimental AFM, ferromagnetic (FM) and another AFM states are compared to obtain the exchange parameters between nearest neighbors of local moments on Fe ions.

3 Results

The ^{57}Fe Mössbauer spectra and fitting parameters for cubic $BaFeO_2F$ were reported earlier [9]. The magnetic ordering temperature was determined as T_N = 645±5K.

3.1 Mössbauer spectra recorded from the hexagonal (6H)- and trigonal (15R)-phases of $BaFeO_2F$ in the temperature range 15 to 300K.

The ^{57}Fe Mössbauer spectra recorded from the hexagonal (6H) phase at 15K, 77K and 300K are shown in Figure 2 and the fitting parameters are listed in Table 1. The spectra recorded from the trigonal (15R) phase at 16K, 69K and 298K are shown in Figure 3 with the fitting parameters listed in Table 2. All the fitted spectral components from both phases showed ordered magnetic structure with values of magnetic hyperfine field (B_{hf}) and isomer shift (δ) characteristic of iron in the Fe^{3+} oxidation state.

In both the 6H and 15R materials all the Mossbauer spectra consist of overlapping sextet components in which one sextet has a significantly higher hyperfine field. This sextet represents the Fe1 site in the 6H compound and the Fe3 site in the 15R compound. In these octahedral sites the Fe ion interacts magnetically with 6 neighbouring Fe ions via the corner anions (the configuration of the 3c cubic material).

In addition to the high field sextet, the spectra of the 6H material show three overlapping sextets with lower hyperfine field assigned to the Fe2 site. In this site the Fe ions interact with three Fe ions via corner anions and with an Fe ion on the nearest Fe2 site via an octahedron face. Additional splitting of the hyperfine field values of these components indicates some randomness around this site, possibly due to a degree of O/F disorder on the neighbouring anion sites.

The occupation ratio of 1:2 for Fe1:Fe2 sites in the structure implies a relative area of 33% for the higher field component. The values shown in Table 1 are not far from this value when account is taken of the difficulty of determining relative areas accurately in spectra with overlapping components. There may, however, be some evidence for a relatively smaller recoil free fraction on the high field site from the relative area of this component in the 300K spectrum.

In the spectra of the 15R material, the lower field sextet components are assigned to the Fe1 and Fe2 sites. The structure implies relative areas of 20%: 40%: 40% for the Fe3: Fe1: Fe2 sites and the values of Table 2 show fair agreement with these values.

The values do, however, lend some additional support for a relatively smaller value of recoil free fraction for the high field component.

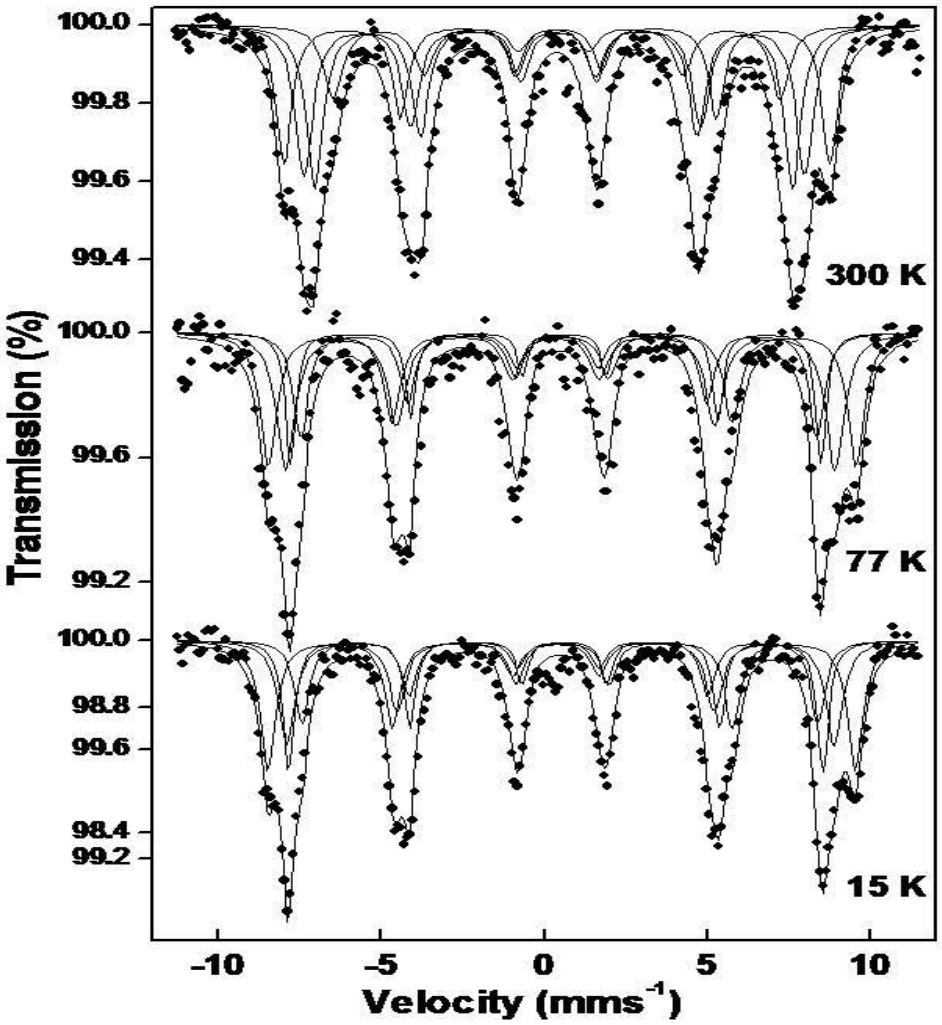

Figure 2. ^{57}Fe Mössbauer spectra recorded from 6H-$BaFeO_2F$ at low temperatures

Table 1. ^{57}**Fe Mössbauer parameters recorded from 6H-BaFeO$_2$F at low temperatures**

Temperature (K)	δ ± 0.02 (mms^{-1})	e^{2}qQ/2 ± 0.02 (mms^{-1})	B ± 0.5 (T)	Relative Area ± 3 (%)
300	0.41	-0.02	51.9	25
	0.36	-0.08	45.5	30
	0.33	-0.02	47.7	29
	0.33	0.05	42.5	16
77	0.54	0.00	55.9	29
	0.48	-0.13	50.4	18
	0.41	0.07	52.3	32
	0.41	0.02	49.1	21
15	0.54	-0.01	55.8	31
	0.48	-0.13	50.8	23
	0.42	0.07	52.1	27
	0.45	0.02	49.1	19

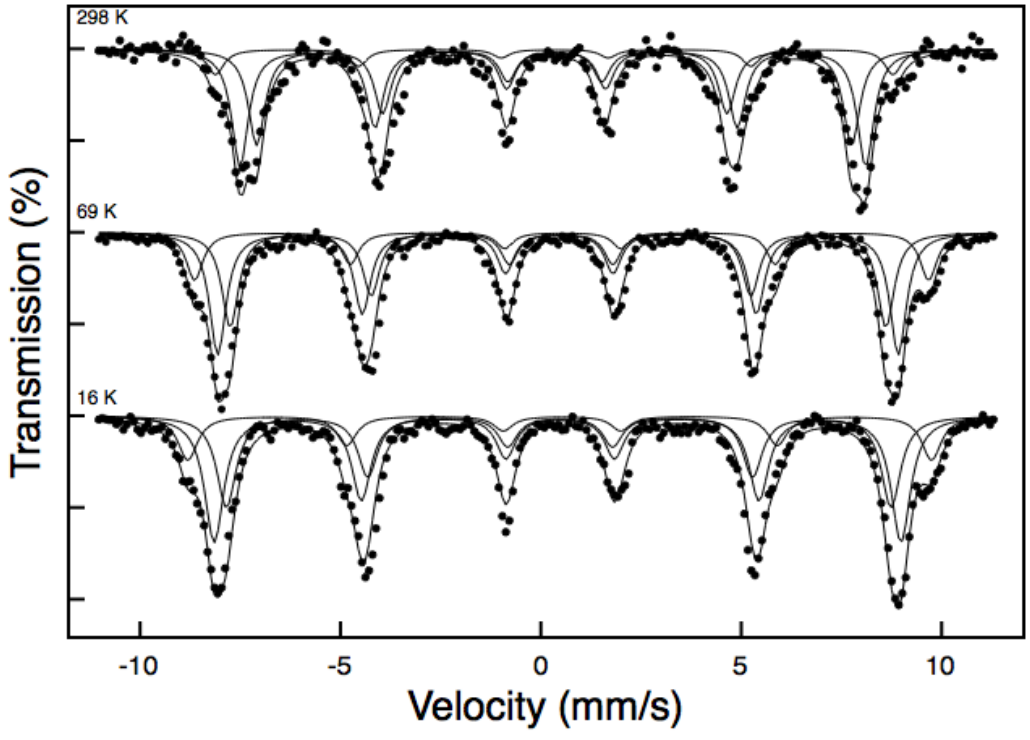

Figure 3. ^{57}**Fe Mössbauer spectra recorded from 15R-BaFeO$_2$F at low temperatures**

Table 2. ^{57}Fe Mössbauer parameters recorded from 15R-$BaFeO_2F$ at low temperatures

Temperature (K)	δ ± 0.02 (mms^{-1})	$e^2qQ/2$ ± 0.02 (mms^{-1})	B ± 0.05 (T)	Relative Area ± 3 (%)
298	0.46	-0.08	52.4	12
	0.33	-0.06	48.4	41
	0.37	-0.02	46.1	47
77	0.53	-0.03	56.8	17
	0.47	-0.08	50.7	36
	0.44	-0.03	52.7	48
16	0.50	-0.06	57.5	18
	0.46	-0.04	51.4	35
	0.45	-0.06	53.1	48

3.2 Determination of magnetic ordering temperature for the hexagonal (6H)- and trigonal (15R)- phases of $BaFeO_2F$

The ^{57}Fe Mössbauer spectra of hexagonal 6H-$BaFeO_2F$ at temperatures of 295K, 473K, 573K, 593K, 597K and 603K are shown in Figure 4 with the fitting parameters listed in Table 3.These spectra are seen to continue to high temperature those spectra shown in Figure 2. Comparison of the fits at 300K/295K in Tables 1 and 3 where the separate series of low temperature and high temperature spectra overlap shows basically the same fit although in the slightly better resolved spectrum at 295K the large intensity sextet with hyperfine field B_{hf} =45.7T replaces the sum of the slightly split components with B_{hf} = 45.5T and 47.5T seen in the 300K spectrum. Overall the fits are consistent with a smooth evolution of the parameters of the spectral components with temperature up to the magnetic ordering temperature.

A graph of average magnetic hyperfine field B_{hf} (T) versus temperature T is shown in Figure 6. In order to extract the value of T_N points evaluated from the expression

$$B_{hf}(T) = B_{hf}(0)[\ 1\text{-}T/T_N]^{\beta}$$

which describes the variation of the mean hyperfine field with temperature as T —>T_N were compared with the experimental points. This expression, valid as T -> T_N, is good for the determination of T_N but less reliable for the value of $B_{hf}(0)$. The best agreement between theoretical and experimental points, shown in Figure 6, was obtained with the values of β = 0.30, $B_{hf}(0)$ = 52.4T and T_N = 597±3K.

Spectra recorded from trigonal 15R-$BaFeO_2F$ at temperatures of 296K, 373K, 473K, 573K, 628K, 635K and 638K are shown in Figure 5 with the fitting parameters listed in Table 4.These spectra continue the variation of the spectra with temperature from those seen in Figure 3. The fitting parameters of these spectra also show a smooth evolution with temperature up to the magnetic ordering temperature. In an analysis similar to that described above the best agreement between theoretical and experimental points, shown in Figure 7, gave values of $\beta = 0.30$, $B_{hf}(0) = 52.4T$ and $T_N = 636\pm3K$.

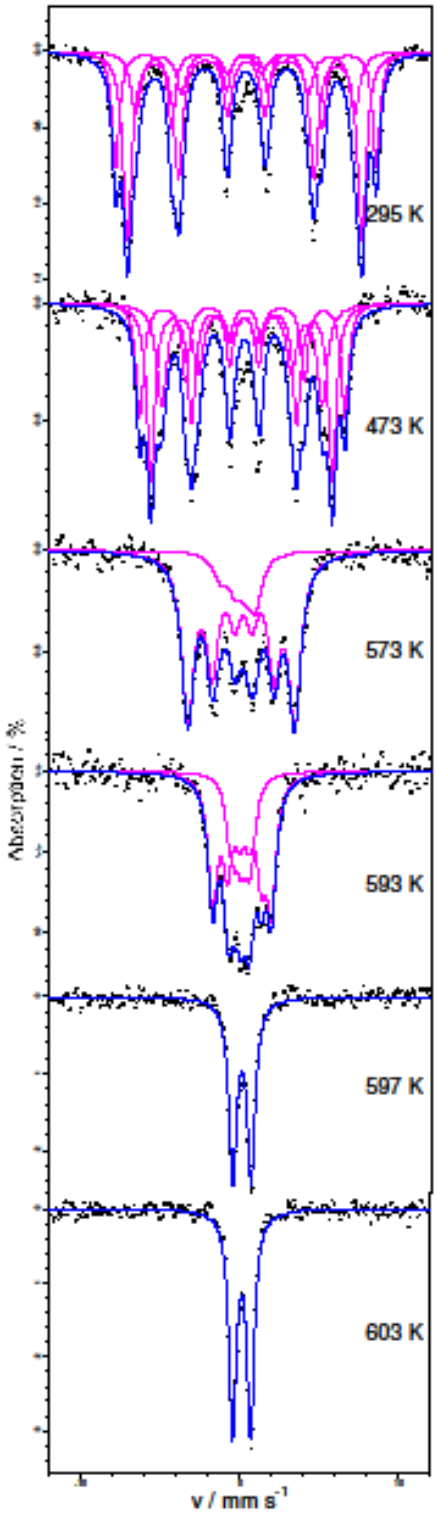

Figure 4. ^{57}Fe Mössbauer spectra recorded from 6H-$BaFeO_2F$ at temperatures above ambient temperature.

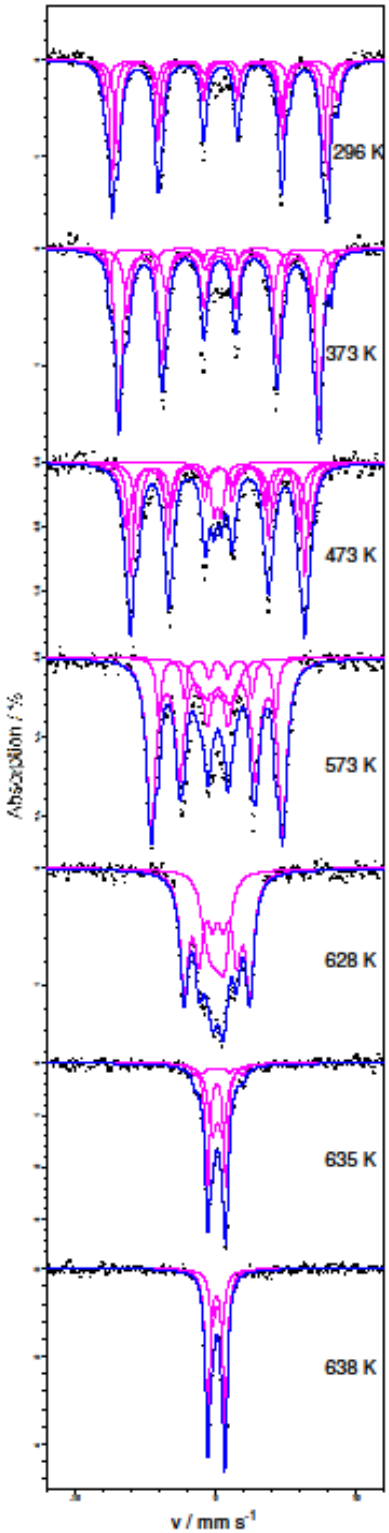

Figure 5. ^{57}Fe Mössbauer spectra recorded from 15R-$BaFeO_2F$ at temperatures above ambient temperature.

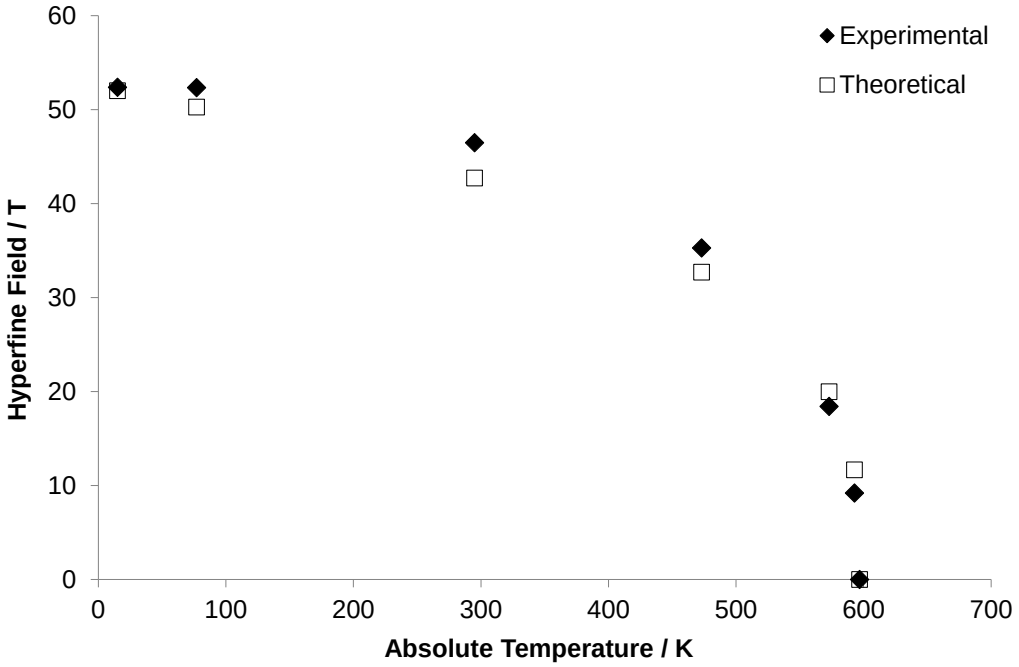

Figure 6. Plot of magnetic hyperfine field as a function of temperature for 6H-$BaFeO_2F$

Table 3. ^{57}Fe Mössbauer parameters recorded above ambient temperature for 6H-$BaFeO_2F$.

Temperature (K)	δ ± 0.02 (mm s^{-1})	$e^2Qq/2$ / Δ ± 0.02 (mm s^{-1})	B ± 0.05 (T)	Relative area ± 2 (%)
295	0.42	-0.06	50.8	27
	0.35	-0.10	45.7	53
	0.33	0.02	42.7	20
473	0.24	-0.16	40.0	26
	0.19	-0.16	35.4	42
	0.22	-0.18	31.3	32
573	0.15	-0.12	20.8	83
	0.12	-0.38	6.8	17
593	0.19	-0.14	11.4	69
	0.08	-0.06	4.3	31
597	0.14	1.15	-	100
603	0.13	1.13	-	100

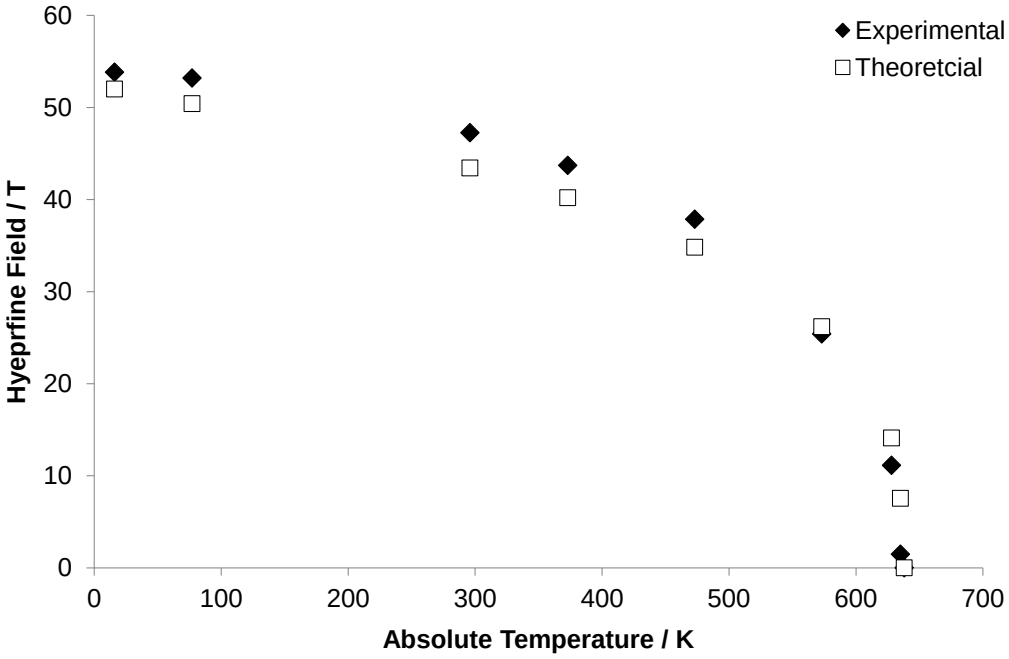

Figure 7. Plot of magnetic hyperfine field as a function of temperature for 15R-$BaFeO_2F$

Table 4. ^{57}Fe Mössbauer parameters recorded above ambient temperature for 15R-$BaFeO_2F$.

Temperature (K)	δ ± 0.02 (mm s^{-1})	$e^2Qq/2$ / Δ ± 0.02 (mm s^{-1})	B ± 0.05 (T)	Relative area ± 2 (%)
296	0.46	-0.06	51.1	20
	0.31	-0.02	47.5	40
	0.36	-0.04	45.1	40
373	0.37	-0.02	48.8	8
	0.28	-0.06	44.2	66
	0.33	0.04	40.9	26
473	0.35	0.02	42.1	7
	0.21	-0.06	38.5	71
	0.30	0.18	34.5	22
573	0.13	-0.06	29.0	71
	0.16	-0.08	25.8	14
	0.12	-0.08	8.0	15
628	0.13	-0.04	14.4	67
	0.08	-0.10	4.5	33
635	0.15	0.18	10.5	12
	0.15	0.74	-	42
	0.09	1.31	-	46
638	0.16	0.67	-	30
	0.09	1.25	-	70

4 Discussion

The preparation of $BaFeO_2F$ in three structural modifications (cubic, hexagonal and trigonal) enables the magnetic properties (including the magnetic ordering temperatures) to be compared as a sole function of the different structural environments and free from considerations of different iron oxidation states.

4.1 Magnetic characteristics of individual structures

In order to facilitate the structural discussion a selection of Fe-Fe bond distances and Fe-X-Fe angles are collected in Table 5. A summary of magnetic moments is contained in Table 6.

Table 5. Selected Fe-Fe bond distances and Fe-X-Fe (X = anion) angles in cubic-, 6H- and 15R-$BaFeO_2F$.

compound		bond distance Fe-Fe [Å]	bond angle Fe-X-Fe [°]
cubic $BaFeO_2F$ [9]	Fe-Fe	4.06	180.0
6H-$BaFeO_2F$ [14]	Fe1 connected to 6 Fe2 via corners (O^{2-})	3.93	173.9
	Fe2 connected to 3 Fe1 via corners (O^{2-})	3.93	173.9
	Fe2 connected to 1 Fe2 via face (F^-)	2.92	85.8
15R-$BaFeO_2F$ [15]	Fe3 connected to 6 Fe1 via corners (O^{2-})	3.93	173.0
	Fe2 connected to 3 Fe2 via corners (O^{2-})	3.80	180.0
	Fe1 connected to 3 Fe3 via corners (O^{2-})	3.93	173.0
	Fe1 connected to 1 Fe2 via face (83% F^- / 17% O^{2-})	2.96	86.3

Table 6. Summary of magnetic moments on Fe^{3+} in cubic-, 6H- and 15R-$BaFeO_2F$ from neutron diffraction data.

compound	site	μ_B
cubic $BaFeO_2F$ [9] at 4.2 K	Fe	3.94
6H-$BaFeO_2F$ [14] at 298 K	Fe1	3.65
	Fe2	3.32
15R-$BaFeO_2F$ [15] at 298 K	Fe1	3.55
	Fe2	3.47
	Fe3	3.97

4.1.1 Cubic $BaFeO_2F$ (*Pm-3m*)

It can be seen in Figure 1a that each Fe^{3+} ion in cubic $BaFeO_2F$ is surrounded by an octahedron of anions. The octahedra are connected via corner sharing of anions. The ^{57}Fe Mössbauer spectra recorded in the magnetically ordered temperature range

consist of a single magnetic sextet with broadened lines [9]. The single sextet arises from the single crystallographic site of the Fe^{3+} ions and the broadening is attributed to the effect of different quadrupole interactions where different configurations of O^{2-} and F^{-} ions in the surrounding anion sites result in different angles between the principal axis of the electric field gradient (EFG) and the magnetic hyperfine field direction. This model gave good fits to the spectra with hyperfine values characteristic of Fe^{3+} ions [9].

4.1.2 Hexagonal 6H-BaFeO2F (*P*6_3*/mmc*)

From Figure 1b the Fe^{3+} ions in this hexagonal structure can be seen to occupy two crystallographically different sites Fe1 and Fe2 with a relative multiplicity ratio of 1:2. The Mössbauer spectra in the magnetically ordered temperature range show magnetic sextet components in which the sextet with the largest value of hyperfine field is partially separated from the other magnetic components. The fitting values of this partially separated sextet (for example at 15K, B_{hf} = 55.8T, δ = 0.54mm/s and relative area = 31%) clearly indicate that this component arises from iron on the Fe1 site which has similar coordination to iron in the cubic compound. The other sextet components, accounting for 69% of the spectral area, arise from the Fe2 site and are characterised by smaller values of B_{hf} and δ. A possible explanation for these smaller values of hyperfine parameters stems from the structural observation that in the Fe2 sites the iron ions are displaced from the centres of their octahedra in the sense of a mutual repulsion between the iron ions. This brings each iron ion closer to the three O^{2-} anions of the octahedron than to the three F^{-} ions which define the common face. Proximity to the O^{2-} ions can lead to a more covalent interaction which will result in the observed smaller values of B_{hf} and δ for these sextet components. This is also in line with the value of the iron magnetic moments for the iron ions in the Fe1 and Fe2 sites determined by room temperature neutron diffraction [14] (Table 6) are 3.65 μ_B and 3.32 μ_B respectively. The relatively short distance (d = 2.92 Å) between Fe ions on the Fe2 sites gives rise to the possibility of direct exchange interaction along the z axis which is discussed below in Section 4.2. Such direct interaction can also result in the formation of partially covalent bonds, which again could be used to explain the lower B_{hf}.

4.1.3 Trigonal 15R-$BaFeO_2F$ (*R-3m*)

In Figure 1c it is seen that the Fe^{3+} ions in this trigonal structure occupy three distinct sites Fe1, Fe2 and Fe3 with relative populations 2:2:1. The Mössbauer spectra in the temperature range of magnetic order show a profile which is well fitted by three sextet components. The component with the largest value of hyperfine field (at 16K B_{hf} = 57.3 T, δ = 0,50mm/s) has a fitted relative area of 18% - close to the 20% expected by identifying this component with the Fe3 site which is connected with six neighbour octahedra via corner sharing O^{2-} ions. The other two sextet components are identified with the Fe1 and Fe2 sites. The areas of these components (which are difficult to determine precisely in the fitting due to the degree of overlap) are consistent with the 40% areas expected from the structure. The smaller values of hyperfine field and isomer shift (at 16K B_{hf} = 51.4 T and δ = 0.46 mm/s) are consistent with the greater degree of covalency of the iron ions in the Fe1 and Fe2 sites as discussed above.

4.2 Magnetic ordering temperatures of cubic, hexagonal and trigonal $BaFeO_2F$

The magnetic ordering temperatures of the cubic, hexagonal and trigonal forms of $BaFeO_2$ F have been found to be 645±5K [9], 597±3K and 636±3K respectively.

The striking feature of these values is their similarity. In these different structures the iron is always present as Fe^{3+} but the differences in crystal structure lead to an expectation of 3D magnetic structure in the cubic phase but a degree of 1D nature in the hexagonal- and trigonal- forms where the magnetic coupling along the z axis is strong but that in the crystallographic a-b plane is weak. In addition the magnetic coupling in the cubic phase is by six 180^0 superexchange pathways via corner sharing O^{2-}anions (as shown in Figure 8a) which is known to give strong antiferromagnetic interaction.

In the hexagonal phase the Fe1 sites interact via six 180^0 superexchange paths (as in the cubic phase) but the Fe2 sites interact with three 180^0 superexchange paths and three 90^0 superexchange paths via the three F^- ions that define the shared face of the adjacent octahedron.

In the trigonal phase the Fe3 site couples via six 180^0 superexchange paths (as in the cubic phase and in the Fe1 site of the hexagonal compound) but the Fe1 and Fe2

sites interact via three 180^0 superexchange paths and three 90^0 superexchange paths.

It is expected that the 90^0 superexchange coupling across the shared face of the adjacent octahedron would be different from the 180^0 coupling of the cubic phase. This should lead to weaker links in the chain of magnetic interactions along the z axis and in appreciable lowering of the magnetic ordering in the hexagonal and trigonal phases from that of the cubic phase.

The experimental result, where only a modest reduction in the magnetic ordering temperatures in the hexagonal and trigonal phases is observed, focusses attention on

(1) the magnetic interaction of the Fe ions across the common face of the adjacent octahedra

(2) the geometrical configuration of the interacting Fe ions in the hexagonal- and trigonal- structures

We consider these aspects in turn.

(1) Magnetic interaction between the Fe sites across a common octahedral face can have two parts (i) 90^0 superexchange proceeding via the three anions that define this face and (ii) direct exchange [22] between the Fe ions

(i) The 90^0 superexchange interaction between Fe^{3+} - O^{2-} - Fe'^{3+} can occur via charge transfer between $Fe(d\varepsilon) \leftrightarrow O(p_\pi)$ and non-orthogonal (antiferromagnetic) exchange (p_σ – $d\gamma'$) as sketched in Figure 8c. Such interactions occur in $MnCl_2$ [23].

(ii) Direct exchange [22] may also occur – arising from the proximity of the Fe ions on Fe2 sites in the 6H phase or the Fe1 and Fe2 sites in the 15R phase. This interaction is sketched in Figure 8b.

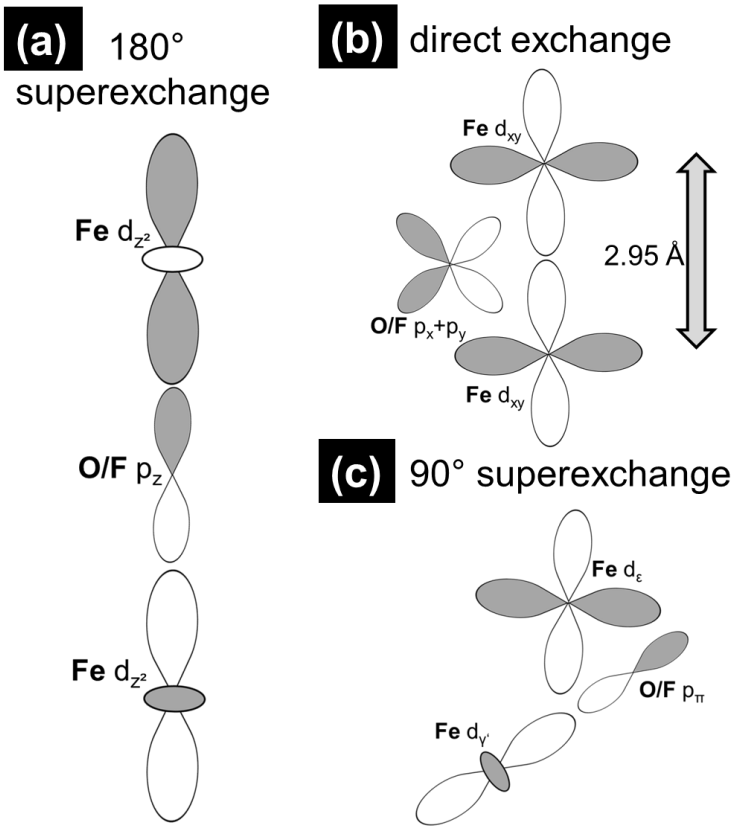

Figure 8. Exchange interactions for (a) corner sharing Fe octahedra and (b) and(c) face sharing octahedra

Accounts of the above mechanisms (i) and (ii) are given in references [23] and [22, 24] respectively. These accounts lead to the expectation of antiferromagnetic coupling by each mechanism for the case where both ions have $3d^5$ high spin configuration. This is in agreement with the observed magnetic structure. An evaluation has been made of the combined strength of these interactions using DFT based calculations (see later in this section), and the experimental result of the similar ordering temperatures indicates that this combined antiferromagnetic interaction must be strong.

(2) In the 6H- structure each Fe2 ion has three strong 180^0 superexchange interactions with Fe1 ions of the neighbouring layer as well as the Fe2 – Fe2 interaction discussed above. The combined effect of these interactions will stabilise the antiferromagnetic structure and limit the reduction in ordering temperature as compared with the cubic phase.

Similar combinations of strong 180^0 superexchange and the 90^0 superexchange and direct exchange interactions occur for the Fe1 and Fe2 site Fe^{3+} ions in the trigonal form which similarly lead to a limited reduction in the magnetic ordering temperature compared to the cubic form.

DFT based calculations can help to understand the distinct magnitudes of exchange interactions arising between face shared- (exchange parameter J_1) and corner shared- octahedra (exchange parameter J_2). In contrast to our expectation, we found that J_1 (0.143 eV) is significantly larger than J_2 (0.046 eV). However, it is important to keep in mind that for c-type layers, one iron atom shares its polyhedron with three neighbouring octahedra via corners. Therefore, the interlayer exchange couplings for octahedra connected via c-type and h-type layers can be calculated to be $J_c = 3\ J_2 =$ 0.138 eV and $J_h = J_1 = 0.143$ eV respectively. Therefore, J_c and J_h must be regarded to be in the same order of magnitude, and this can serve to explain why the magnetic ordering temperatures are similar for the three modifications (cubic-, 6H- and 15R-$BaFeO_2F$).

Robust antiferromagnetism in some fluorinated hexagonal perovskites has been reported [19] but in these compounds, 6H-$Ba_{0.8}Sr_{0.2}FeF_xO_{3-\delta}$ and 15R-$BaFeF_xO_{3-\delta}$, the high magnetic ordering temperatures are associated with fluorination causing major structural changes that enhance the magnetic coupling, e. g. ordering of anion vacancies within the hexagonal- type layers resulting in corner sharing of tetrahedra connecting the iron ions between those hexagonal- type layers. In the phases of $BaFeO_2F$ examined here fluorination gives completely filled anion sublattices with octahedral coordination, while additionally assuring an oxidation state of +3 for all the Fe ions. In these present systems it is the effect of the different interconnection of octahedra (face-sharing vs. corner-sharing) that define the magnetic coupling mechanisms that are responsible for the differences in magnetic ordering temperatures in the different forms of $BaFeO_2F$.

It is noted that the magnetic ordering temperatures of the 6H- $BaFeO_2F$ (597 ± 3 K) and the 15R – BaFeO2F (636 ± 3K) are significantly different. A major difference between those two phases lies in the fact that for the 15R phase the hexagonal layers cannot only contain fluoride ions, but also must contain some oxide ions at least partially regarding a simple consideration of stoichiometry (12*k* (c-type) and 6*h* (h-type) anion sites for the 6H compound vs. 18*h* and 9*e* (both c-type) as well as 18*h*

(h-type) anion sites for the 15R compound). Although this structure is too large to be calculated by means of DFT methods, we assume that a partial composition of the h-type layers by oxide ions might result in slightly more robust exchange interactions between cations connected via such layers and therefore an increased ordering temperature by about 40 K.

5 Conclusions

The ^{57}Fe Mössbauer spectra recorded from the cubic-, hexagonal- and trigonal modifications of $BaFeO_2F$ can be related to the structural characteristics surrounding the Fe^{3+} sites in these materials. The similarity in the magnetic ordering temperatures of the three modifications can be explained by the details of the magnetic interactions between the Fe^{3+} sites in the three materials.

6 Acknowledgements

Oliver Clemens thanks the German Academic Exchange Service (DAAD) for being given a Postdoctoral Research Fellowship and the German Science Foundation for providing an Emmy Noether Research Fellowship (Grant No. CL 551/2-1). We acknowledge financial support from Spanish MINECO (Project MAT2015-64110-C2-1-P).

7 References

[1] Francesconi M G and Greaves C 1997 Anion substitutions and insertions in copper oxide superconductors *Supercond. Sci. Technol.* **10** A29

[2] Greaves C and Francesconi M G 1998 Fluorine insertion in inorganic materials *Curr. Opin. Solid State Mater. Sci.* **3** 132-6

[3] McCabe E E and Greaves C 2007 Review: Fluorine insertion reactions into pre-formed metal oxides *J. Fluorine Chem.* **128** 448-58

[4] Clemens O and Slater P R 2013 Topochemical modifications of mixed metal oxide compounds by low-temperature fluorination routes *Rev. Inorg. Chem.* **33** 105-17

[5] Berry F J, Ren X, Heap R, Slater P and Thomas M F 2005 Fluorination of perovskite-related $SrFeO_{3-d}$ *Solid State Commun.* **134** 621-4

[6] Berry F J, Heap R, Helgason Ö, Moore E A, Shim S, Slater P R and Thomas M F 2008 Magnetic order in perovskite-related $SrFeO_2F$ *J. Phys.: Condens. Matter* **20** 215207

[7] Clemens O, Haberkorn R, Slater P R and Beck H P 2010 Synthesis and characterisation of the $Sr_xBa_{1-x}FeO_{3-y}$-system and the fluorinated phases $Sr_xBa_{1-x}FeO_2F$ *Solid State Sci.* **12** 1455-63

[8] Heap R, Slater P R, Berry F J, Helgason O and Wright A J 2007 Synthesis and structural determination of the new oxide fluoride $BaFeO_2F$ *Solid State Commun.* **141** 467-70

[9] Berry F J, Coomer F C, Hancock C, Helgason Ö, Moore E A, Slater P R, Wright A J and Thomas M F 2011 Structure and magnetic properties of the cubic oxide fluoride $BaFeO_2F$ *J. Solid State Chem.* **184** 1361-6

[10] Clemens O, Haberkorn R, Slater P R and Beck H P 2010 Synthesis and characterisation of the SrxBa1-xFeO3-y-system and the fluorinated phases SrxBa1-xFeO2F *Solid State Sci.* **12** 1455-63

[11] Clemens O, Berry F J, Wright A J, Knight K S, Perez-Mato J M, Igartua J M and Slater P R 2013 A neutron diffraction study and mode analysis of compounds of the system $La_{1-x}Sr_xFeO_{3-x}F_x$ (x=1, 0.8, 0.5, 0.2) and an investigation of their magnetic properties *J. Solid State Chem.* **206** 158-69

[12] Clemens O, Berry F J, Wright A J, Knight K S, Perez-Mato J M, Igartua J M and Slater P R 2015 Reply to “Structural and magnetic behavior of the cubic oxyfluoride $SrFeO_2F$ studied by neutron diffraction” *J. Solid State Chem.* **226** 326-31

[13] Slater P R 2002 PVDF as a reagent for the synthesis of K_2NiF_4-related inorganic oxide fluorides *J. Fluorine Chem.* **117** 43-5

[14] Clemens O, Wright A J, Berry F J, Smith R I and Slater P R 2013 Synthesis, structural and magnetic characterisation of the fully fluorinated compound 6H-$BaFeO_2F$ *J. Solid State Chem.* **198** 262-9

[15] Clemens O, Berry F J, Bauer J, Wright A J, Knight K S and Slater P R 2013 Synthesis, structural and magnetic characterisation of the fluorinated compound 15R-$BaFeO_2F$ *J. Solid State Chem.* **203** 218-26

[16] Müller U 2004 *Anorganische Strukturchemie* (Wiesbaden: B. G. Teubner Verlag)

[17] Clemens O, Groeting M, Witte R, Manuel Perez-Mato J, Loho C, Berry F J, Kruk R, Knight K S, Wright A J, Hahn H and Slater P R 2014 Crystallographic and Magnetic Structure of the Perovskite-Type Compound $BaFeO_{2.5}$: Unrivaled Complexity in Oxygen Vacancy Ordering *Inorg. Chem.* **53** 5911-21

[18] Sturza M, Daviero-Minaud S, Kabbour H, Gardoll O and Mentré O 2010 Fluorination of Iron Hexagonal Perovskites Promoting Low Temperature Oxygen Mobility *Chem. Mater.* **22** 6726-35

[19] Sturza M, Kabbour H, Daviero-Minaud S, Filimonov D, Pokholok K, Tiercelin N, Porcher F, Aldon L and Mentré O 2011 Unprecedented Robust Antiferromagnetism in Fluorinated Hexagonal Perovskites *J. Am. Chem. Soc.* **133** 10901-9

[20] Blaha P, Schwarz K, Madsen G K H, Kvasnicka D and Luitz J 2001 *WIEN2k, An Augmented Plane Wave + Local Orbitals Program for Calculating Crystal Properties* (Techn. Universität Wien, Austria

[21] Perdew J P and Wang Y 1992 Accurate and simple analytic representation of the electron-gas correlation system *Phys. Rev. B* **45** 13244-9

[22] Goodenough J B 1960 Direct Cation- -Cation Interactions in Several Oxides *Physical Review* **117** 1442-51

[23] Suzuki M and Suzuki I 2009 *Lecture on Superexchange* (Binghampton: State University of New York)

[24] Goodenough J B 1963 *Magnetism and the Chemical Bond* (New York: Interscience Publisher)